Preprints of the 21st IFAC World Congress (Virtual)
Berlin, Germany, July 12-17, 2020

Data-Driven Modelling of the Nonlinear Cortical Responses Generated by Continuous Mechanical Perturbations

Hasan A. Nozari*, Z. Rahmani*, Paolo Castaldi, S. Simani***, S.J. Sadati***
** Faculty of Electrical and Computer Engineering, Babol Noshirvani University of Technology, Babol, Iran (e-mail: hanozari@nit.ac.ir, zrahmani@nit.ac.ir, j.sadati@nit.ac.ir)*
*** Department of Electrical, Electronic and Information Engineering, University of Bologna, Via Fontanelle40, (FC), 47121, Italy Forlí (e-mail: paolo.castaldi@unibo.it)*
****Department of Engineering, University of Ferrara, Via Sargat, IE-44122 Ferrara (FE), Italy (e-mail: ilvio.simani@unife.it)*

Abstract: Cortical responses to external mechanical stimuli recorded by electroencephalography have demonstrated complex nonlinearity with fast dynamics. Hence, the modelling of the human nervous system plays a crucial role in studying the function of the sensorimotor system and can help in disentangling the sensory-motor abnormalities in functional movement disorders. In this paper, a non-parametric model is estimated based on locally-linear neuro-fuzzy structures trained by an evolutive algorithm relying on locally-linear model-tree. In particular, simulation model as well as a multi-step ahead predictor model is considered to describe the nonlinear dynamics governing the cortical response. The proposed modelling method is applied to an experimental dataset representing brain activities from ten young healthy subjects. These electroencephalography signals are recorded while robotic manipulations have been applied to their wrist joints. The obtained results are satisfactory and are also compared to those achieved with different modelling strategies applied to the same benchmark data.

Keywords: Locally linear neuro-fuzzy network, locally linear model-tree, cortical response, electroencephalography signals.

1. INTRODUCTION

The neural control of healthy movement involves proprioceptive information from the periphery to reach the cortex; this sensory information is needed for creating internal models allowing accurate movement planning (feed-forward control) and for generating suitable responses to disturbances (feedback control). It is well established that the link between a movement and the cortical reaction increases the understanding of the sensorimotor system and helps to solve sensorimotor problems in movement disorders (Vlaar et al., 2018). The analysis of the dynamics between the integration of sensory system and motor system allows to generate a continuous proprioceptive excitation. Moreover, it is widely available a high-precision technique for recording brain activities such as ElectroEncephaloGraphy (EEG) or magnetencephalography. To this end, external manipulation of wrist or finger as a continuous stimulus allows for steady-state study of the nervous system since it is consistently involved in processing the sensory signals.

Taking into account that human nervous system consists of multiple neuronal networks, this process is considered as a complex nonlinear closed-loop system with abrupt variation of its dynamics (Campfens et al., 2013 and Yang et al., 2016a). Therefore, the use of linear modelling techniques (Campfens et al., 2013 and Vlaar et al., 2017) can provide only limited information on the behaviour of this system; as an example, the linear approach to model the relation between proprioceptive stimulus and evoked cortical response can only capture 10% of the brain activity (Vlaar et al., 2017. However, little research efforts have been devoted to nonlinear modelling of the cortical response. On the other hand, a few researches have employed nonparametric nonlinear modelling approaches based on Volterra series to capture the nonlinear dynamics of brain response to joint stimuli (Vlaar et al., 2018 and Tian et al., 2018). This strategy only explained around 40% of the measured EEG signals. The major drawback of the Volterra based methods is that the model output depends merely on the previous values of the process inputs. In order to manage this limitation, other works have considered Nonlinear AutoRegressive Moving Average with eXogenous inputs (NARMAX) prototypes to capture the dynamics of cortical response (Tian et al., 2018). It is worth noting the complex behaviour of the human nervous system that includes sub-harmonics, fast dynamics, bifurcations, and even chaos (Breakspear, 2017 and Yang et al., 2016b)- Therefore, the problem of nonlinear modelling of the human nervous system still requires more investigations.

This study suggests employing Locally Linear Neuro-Fuzzy (LLNF) networks for capturing the nonlinear dynamics from the cortical response to the mechanical stimulations. The main goal is to extract as much information as possible about the system from given data, without using any prior knowledge. In this study, LLNF models are computed by using local AutoRegressive with eXogenous inputs (ARX), AutoRegressive Moving Average with eXogenous inputs (ARMAX), Output Error (OE), and Volterra structures (Nelles, 2001). It is worth noting that the transparent architecture of the LLNF models can enhance to understand he highly nonlinear relationship between the mechanical stimulus and cortical response.

The remainder of this paper is organised as follows. Section 2 provides the overall description of the developed setup and the data acquisition system. In Section 3, the proposed nonlinear modelling approaches are presented. In particular, Section 3.1 introduces the proposed simulator and predictor models, whilst Section 3.2 addresses the structure of the LLNF system Section 4 presents the achieved simulation results and some related discussions. Finally, concluding remarks and open problems are drawn in Section 5.

2. EXPERIMENTAL SETUP DESCRIPTION

Ten physically healthy and right-handed young individuals aged between 22 and 25 years (5 males) were involved in the experiments. The experimental procedure was approved by the Human Research Ethics Committee of the Delft University of Technology (TU Delft), the Netherlands. All subjects provided written knowledgeable consent before participating in experiments. During the test, the subjects were sat with their right forearm placed on an armrest while their hand was fixed to the handle of a robotic manipulator (Wristalyzer, MOOG Inc., The Netherlands). Multisine perturbations were applied to the participants as flexion and extension stretches via the handle of the manipulator, thus representing the external inputs to the nervous system. Subjects were suggested to relax their arm and joints, and not react to the stimuli generated by robotic manipulator.

These stimuli represent the sum of sinusoids with odd harmonics of the fundamental frequency of 1, 3, 5, 7, 9, 11, 13, 15, 19, and 23Hz and with the period of 1 s. Therefore, seven different realizations of a multisine signal with similar frequencies were created. All perturbation signals have identical statistical distributions with the same root-mean-square of 0.02 radians. The stimulation signals were applied to wrist joints as angular position perturbations; therefore, signal magnitude is expressed in radians. Moreover, these signals were designed to have similar power on the first three frequency components and a dwindling power spectrum (−20dB/decade slope) for higher frequencies. This choice represents a trade-off between the reduced predictability of the input signals (in order to prevent possible predictions by the subjects) and the capabilities of the wrist-manipulator system (Vlaar et al., 2017). Each signal was applied to stimulate the wrist joints for 7 trials of 36 s.

The EEG response was measured from the human nervous system, using an EEG cap with 128 Ag/AgCl electrodes (arranged based on 5/10 system, WaveGuard, ANT Neuro, Germany). The cortical response was sampled at 2048Hz using a Refa amplifier (Twente Medical Systems International B.V., the Netherlands) and recorded for additional analysis. Three seconds were removed from the beginning and the end of each dataset in order to reduce the transient effects, thus resulting in 210 periods for each of the 7 realizations (Vlaar et al., 2018). The dataset is provided in 3 different sizes, namely small (<1MB), medium (around 500MB), and large (around 60GB) and can be accessed through this website (http://www.nonlinearbenchmark.org/). As the first data set (the smallest one) was used in this work; the same dataset was also used for comparison purpose.

3. NONLINEAR SYSTEM IDENTIFICATION

3.1. Simulation and prediction Techniques

Nonlinear dynamic system identification can be carried out by exploiting simulation and prediction model techniques (Nelles, 2002). The structure of the nonlinear predictor and simulator based on local ARX and ARMAX models is depicted in Fig. 1. The simulation model is fed by the past values of the process inputs and the past values of the outputs of the model itself, in order to simulate its future outputs., On the other hand, the one-step ahead prediction model uses the past values of the process inputs and the past process outputs. Fig. 1 represents the structure of the prototype for the prediction and the simulation tasks. In this way, as highlighted in Fig. 1, the model dynamics are included into the nonlinear static approximator through a bank of external tapped delays.

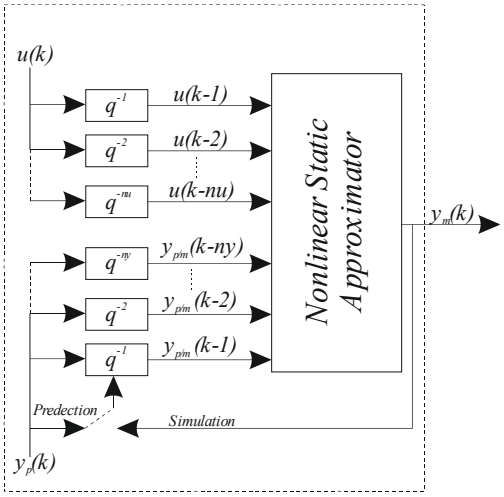

Fig. 1. Nonlinear model with external dynamics for prediction and simulation purposes.

For the identification of nonlinear dynamic systems based on simulation technique, the nonlinear OE structure is given as follows (Billings, 2013):

$$y_m(k) = f(\underline{X}) = f\begin{pmatrix} u(k-1), u(k-2), ..., u(k-nu), \\ y_m(k-1), y_m(k-1), ..., y_m(k-ny) \end{pmatrix} \quad (1)$$

On the other hand, the NARX and NARMAX structures used for one-step ahead prediction are formulated as follows (Billings, 2013):

$$y_m(k) = f(\underline{X}) = f\begin{pmatrix} u(k-1), u(k-2), ..., u(k-nu), \\ y_p(k-1), y_p(k-1), ..., y_p(k-ny) \end{pmatrix} \quad (2)$$

$$y_m(k) = f\begin{pmatrix} u(k-1), u(k-2), ..., u(k-nu), y_p(k-1), ..., y_p(k-ny), \\ e(k-1), e(k-2), ..., e(k-ne) \end{pmatrix} \quad (3)$$

u is the system input, e is the prediction error, y_p and y_m are the system and model outputs, respectively; nu, ny, ne are the number of lags for input, output and the prediction error, respectively. Note that NARMAX model without output dynamics lead to the Volterra structure (Brockett, 1976). On the other hand, a long-term predictive model is characterized by its prediction capabilities over longer prediction horizons (*i.e., h*-steps ahead). Therefore, the structure of a long-term (multistep) predictor model is obtained by means of a series

connection of identical NARX models with the prediction horizon of *h*, as illustrated in Fig. 2.

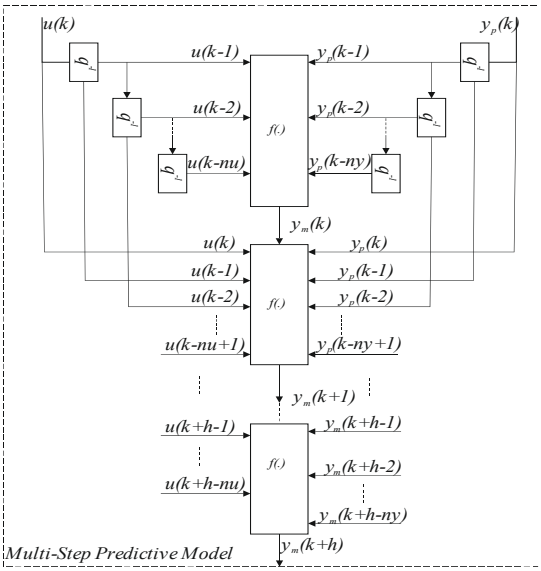

Fig. 2. Architecture of a multi-step NARX predictor model for prediction horizon of h.

According to the structure of the multi-step NARX predictor model of Fig. 2, the *h*-step ahead prediction of the output for a NARX model can be computed as follows:

$$y_m(k+h) = f\begin{pmatrix} u(k+h-1),\ldots,u(k+h-nu), y_m(k+h-1), y_m(k+h-2),\ldots, \\ y_p(k+h-ny) \end{pmatrix} \quad (4)$$

Moreover, the *h*-step ahead prediction using a NARMAX model is described as follows:

$$y_m(k+h) = f\begin{pmatrix} u(k+h-1),\ldots,u(k+h-nu), \\ y_m(k+h-1), y_m(k+h-2),\ldots, \\ y_p(k+h-ny), e(k),\ldots,e(k+h-ne) \end{pmatrix} \quad (5)$$

3.2. Locally linear neuro-fuzzy network

The LLNF models allow to reduce the dimension of the nonlinear input space by using locally linear subspaces. The fuzzy validity functions define the effectiveness of each local linear model in its regions via fuzzy neurons. Each neuron represents a Local Linear Model (LLM), whose effectiveness is determined by its validity function. The LLNF model can be simply inferred as Takagi-Sugeno (TS) fuzzy model, whose rules are represented by neurons; the validity functions correspond to the rule premises, whilst the LLMs represent the rule consequents (Nelles, 2001). The structure of the LLNF model is shown in Fig. 3.

As an example, the overall output of a multi-input single-output LLNF model with NARX structure (*i.e.*, in form of predictor/simulator model) for *D* inputs is represented as follows:

$$y_m(k) = \sum_{j=1}^{M} \begin{bmatrix} b_{j1}u(k-1) + b_{j2}u(k-2) + \ldots + \\ b_{jm}u(k-m) + a_{j1}y_{p/m}(k-1) + \ldots + \\ a_{jn}y_{p/m}(k-n) + \xi_j\varphi_j(\underline{X}) \end{bmatrix} \quad (6)$$

where $y_{p/m}$ denotes the system or the model output, b_{jim_i} and a_{jn} represent the numerator and denominator coefficients respectively, ξ_j is the offset of the LLM$_j$.

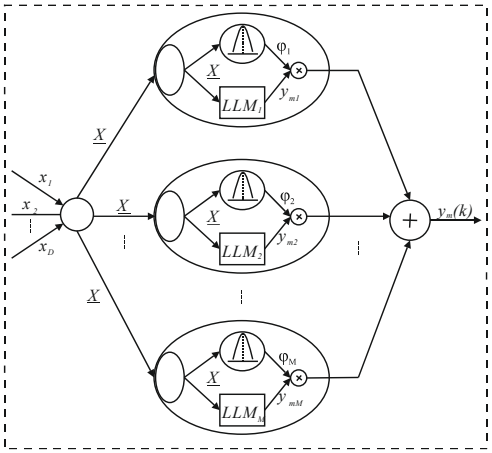

Fig. 3 The general structure of the LLNF model.

Furthermore, the function $\varphi_j(X)$ represents the operating point dependent weighting factor. The parameter vector for the *j*-th LLM is described by the following parameter vector:

$$\underline{w}_j = \left[b_{j1}, b_{j2}, \ldots, b_{jm}, a_{j1}, \ldots, a_{jn}, \xi_j\right]^{\mathrm{T}} \quad (7)$$

A weighted least-squares solution is employed to estimate the parameters for the *j*-th local output. It is noteworthy noting that a LLM is valid only in the region where the associated validity function is close to 1. That is, the validity functions of *u* are typically chosen as normalized Gaussian functions, such that the following relation holds:

$$\sum_{j=1}^{M} \varphi_j(\underline{X}) = 1 \quad (8)$$

The validity functions are chosen as normalized Gaussian functions:

$$\varphi_j(\underline{X}) = \frac{\mu_j(\underline{X})}{\sum_{j=1}^{M} \mu_j(\underline{X})}$$

$$\mu_j(\underline{X}) = exp\left(-\frac{1}{2}\left(\frac{(x_1 - c_{j1})^2}{\sigma_{j1}^2} + \ldots + \frac{(x_D - c_{jD})^2}{\sigma_{jD}^2}\right)\right) = \quad (9)$$

$$exp\left(-\frac{1}{2}\left(\frac{(x_1 - c_{j1})^2}{\sigma_{j1}^2}\right)\right) \times \ldots \times exp\left(-\frac{1}{2}\left(\frac{(x_D - c_{jD})^2}{\sigma_{jD}^2}\right)\right)$$

where the parameters c_{ji} and σ_{ji} represent the centre and the standard deviation of the *j*-th LLM, respectively.

The divide-and-conquer strategy is exploited for finding determining the optimal network structure as it represents the most powerful approach for the LLNF modelling approach. Moreover, the parameters of the validity functions are tuned by means of an evolutive algorithm, namely the LOcally LInear MOdel Tree (LOLIMOT), which divides the input space through axis-orthogonal splits (Nelles, 1996). This algorithm contains an outer loop, where the parameters of the validity functions are determined, and an inner loop, in which the parameters of LLMs are optimised by the weighted least square estimation (Nelles, 1996; Nelles, 2001). The

following pseudo-code was proposed by the authors in order to implement the LOLIMOT algorithm (Nozari et al. 2014):

$c1 \leftarrow Minimum(X)+(Maximum(X)-Minimum(X))/2;$
$\sigma 1 \leftarrow Maximum(X) - Minimum(X)/3;$
$\varphi 1 \leftarrow Calculate(c1, \sigma 1, X)$,$w1 \leftarrow Least\ Square\ (\varphi 1, X, y);$
$y_{m_{LLM_1}} \leftarrow \underline{X} \times \underline{w}$; $y_m \leftarrow y_{m_{LLM_1}} \times \varphi_1$; $e \leftarrow J(y - \hat{y})$; $e_{Local_{LLM_1}} \leftarrow \varphi_1 \times e$; $e_{Local} \leftarrow e_{Local_{LLM_1}}$
For $i=1$ *to* LLM_{max}
  ($Neuron_{new}$, $Neuron_{del}$) ← *Delete Worst Neuron* ($Neuron_{del}$, e_{local})
    For $l=1$ *to Input Dimensions*
      (Split Dimension) ← *Find min-max bounds*($Neuron_{del}$)
      (c_{new}, σ_{new}) ← *Create new neuron;*
      Insert To Model (c_{new}, σ_{new}, *Split Dimension);*
      For $k=1$ *to* $i+1$
        $\varphi_k \leftarrow Calculate(c_k, \sigma_k, X);$
        $w_k \leftarrow Least\ Square(\varphi_k, X, y);$
        $y_{m_{LLM_k}} \leftarrow \underline{X} \times \underline{w}$
      End of k For
      $y_m \leftarrow y_{m_{LLM}} \times \varphi_l$; $e_l \leftarrow J(y_p - y_m)$
      $e \leftarrow$ *Select minimum cost neuron*(e_l);
    End of l For
    IF $e_l <$ *Error Goal*
      Break;
    For $k=1$ *to* $i+1$
      $e_{Local_{LLM_k}} \leftarrow \varphi_k \times e$
    End of k For
End of i For

4. RESULTS AND DISCUSSION

Since 7 multisine realizations are available in the data, initial training phases with cross-validation stages are iteratively carried out (Vlaar et al., 2018). 6 of these date-sets have been used for training (estimating) the model, whilst the remaining one has been exploited for validating the obtained structure. The cross-validation procedure (Stone, 1974) has been repeated 7 times, thus yielding to 7 models for each participant. Therefore, the average performance has been calculated through 7 repetitions for each participant, thus representing the overall performance of the proposed model. These performances have been evaluated by using the Variance Accounted For (VAF) index with a cross-validation test (Tian et al., 2018):

$$VAF = \left[1 - \frac{\mathrm{var}(y_m - y_p)}{\mathrm{var}(y_p)}\right] \times 100 \qquad (10)$$

where y_m represents the model output and y_p represents the system output. Fig. 4 reports one period of the measured and estimated output signals for participant P1. The estimated output signals from the single-step and multi-step (*i.e.*, three-step and eleven-step) ahead predictions using the proposed LLNF-NARX and LLNF-NARMAX models are reported for comparison purpose. Besides, the behaviours of the simulator (NOE) and the Volterra models are also shown with respect to real output signal. Note that both the LLNF-NARX and the LLNF-NARMAX models exhibit good tracking capabilities for the one-step ahead prediction. However, as the prediction horizon increases, the performance of the LLNF-NARMAX model deteriorates, particularly during the eleventh-prediction step. The performance of the Volterra and the NOE models cannot be compared to the predictor models in terms of tracking.

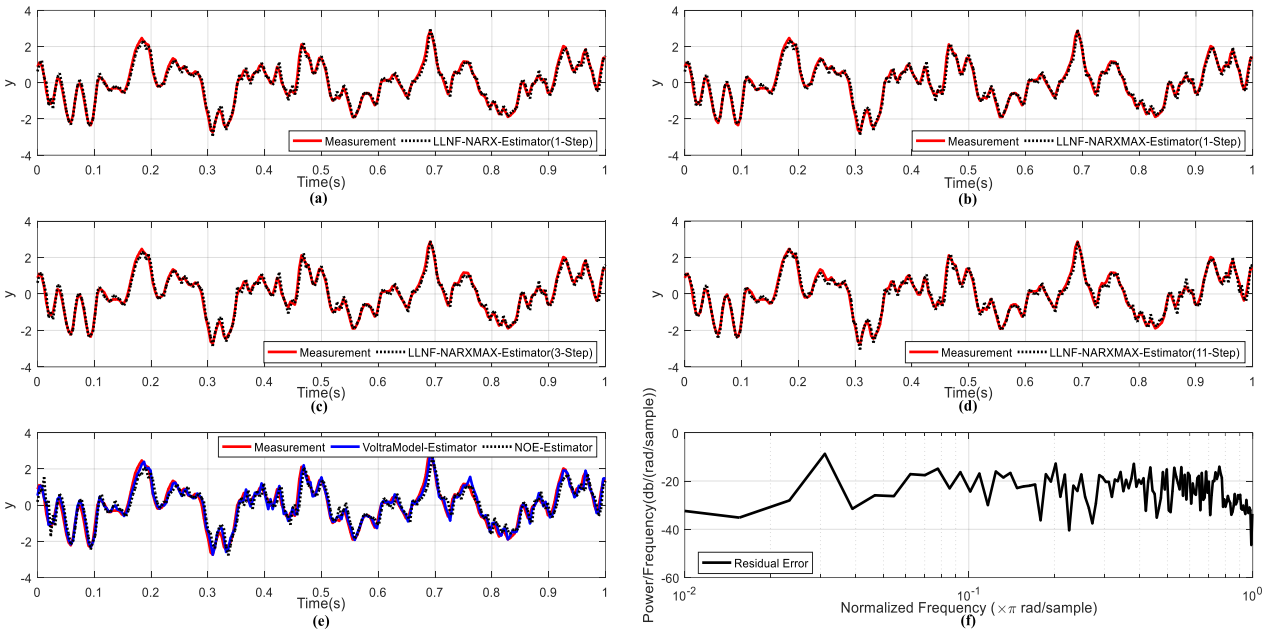

Fig. 4 Performance of the proposed LLNF models for participant P1:(a) one-step ahead prediction by the LLNF-NARX model, (b) one-step ahead prediction by the LLNF-NARMAX model, (c) three-step ahead prediction by the LLNF-NARMAX model, (d) 11-step ahead prediction by the LLNF-NARMAX model, (e) Simulator and Volterra Models, (f) Power spectrum density of the one-step ahead prediction residual for the LLNF-NARMAX model.

predictions using the proposed LLNF-NARX and LLNF-NARMAX models are reported for comparison purpose. Besides, the behaviours of the simulator (NOE) and the Volterra models are also shown with respect to real output signal. Note that both the LLNF-NARX and the LLNF-NARMAX models exhibit good tracking capabilities for the one-step ahead prediction. However, as the prediction horizon increases, the performance of the LLNF-NARMAX model deteriorates, particularly during the eleventh-prediction step. The performance of the Volterra and the NOE models cannot be compared to the predictor models in terms of tracking.

It is clear that the Volterra model estimates the output signal more accurately than the NOE model, as the former exploits

the feedback of the prediction error as input. On the other hand, the one-step ahead residual error for the LLNF-NARMAX model is higher in the high-frequency components within the band of interest. This problem is probably due to the fast dynamics of the EEG oscillation, which can be considered as a measurement noise in the system. In addition, since the average behaviour of the residual error is constant, the residual error can be considered as white noise, thus proving the goof fit of the considered model.

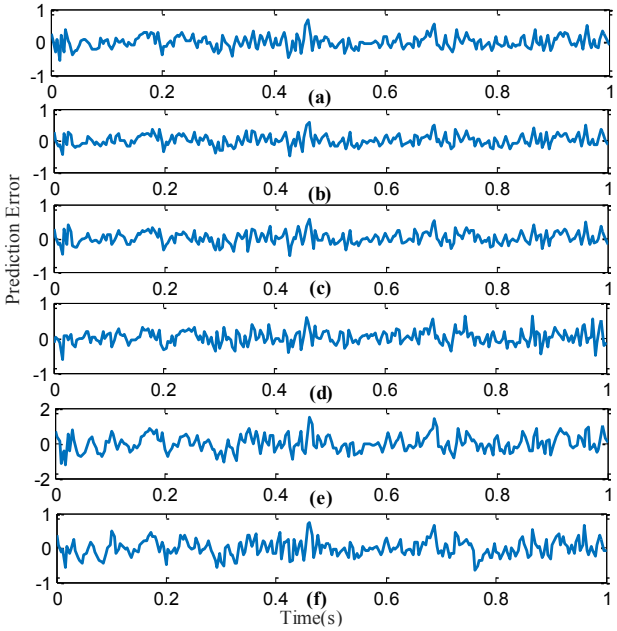

Fig. 5 Prediction errors of proposed models for participant P1: (a) LLNF-NARX model (one step ahead), (b) LLNF-NARMAX model (one step ahead), (c) LLNF-NARMAX model(three step ahead), (d) LLNF-NARMAX model(eleven step ahead), (e) Volterra model, and (e) simulator model.

Fig. 5 reports the variations of the prediction errors over one period for participant P1. As it can be seen, the prediction errors for the NARX and the NARMAX models are around zero, thus highlighting their capabilities to track the measured system outputs with good accuracy. Moreover, the prediction errors generated by the NOE and the Volterra models are significantly different from zero in some intervals, due to their limitations to emulate the EEG response signal. The structures of the proposed LLNF models for a typical tested participant (P1) are summarized in Table 1. The model structure has been obtained by performing an exhaustive search (Eduardo et al, 2001) among all possible model structures, and selecting the model which minimizes the VAF index.

Table 1. Structures of the proposed LLNF-based models for participant P1

		Fold1	Fold2	Fold3	Fold4	Fold5	Fold6	Fold7
LLNF-NARX	nu	2	5	6	2	4	10	2
	ny	10	10	10	5	10	5	10
LLNF-NARMAX	nu	2	5	8	2	1	2	2
	ny	10	10	10	1	8	10	8
	ne	6	4	6	9	6	3	10
LLNF-NOE	nu	2	7	10	2	2	3	7
	ny	9	10	10	5	10	8	5
LLNF-Volterra	nu	1	3	1	1	1	1	3
	ne	10	10	10	8	5	5	10

The performances of the proposed models are reported in the Table 2 for all tested participants. As it can be seen, the LLNF-NARX (93.39% ± 1.71%) and LLNF-NARMAX (94.52% ± 1.45%) one-step ahead prediction models provide the best results, when compared to the LLNF-Volterra (91.27% ± 1.95%) and the LLNF-NOE (68.43 % ± 7.18%) models. Furthermore, as the prediction horizon increases up to 11, the LLNF-NARMAX (86.78% ± 4.50%) model provides better long-term prediction than the LLNF-NARX model (83.56% ± 3.89%). However, it can be noted that increasing the prediction step leads to reduce the prediction performances for both models. This can be due to the fact that the performance of the prediction model tends to those of the simulation model when the prediction horizon increases. It is also worth noting that the eleven-step ahead prediction forecasts 43ms ahead of the cortical response (based on the 256Hz sampling rate), which seems sufficient for evaluating the performance of the proposed models due to the fast dynamics of the human brain.

Table 2 Performances of the proposed LLNF-based models based on the VAF [%] index.

	LLNF-NARX			LLNF-NARMAX			NOE	Volterra.
	Step-1	Step-3	Step-11	Step-1	Step-3	Step-11		
P1	95.49	95.06	88.27	96.22	95.68	83.73	77.95	94.15
P2	92.94	92.05	80.64	93.67	92.79	86.55	62.81	90.68
P3	93.52	92.59	76.85	94.47	93.93	89.23	64.05	90.66
P4	91.82	90.92	84.55	93.55	92.39	87.80	63.29	88.53
P5	94.86	93.38	81.11	95.72	94.98	91.41	73.44	92.54
P6	93.60	93.39	84.58	94.63	91.90	84.70	74.04	92.10
P7	94.49	88.63	82.12	95.74	95.36	91.73	74.52	92.26
P8	90.10	89.55	84.30	91.85	89.75	78.73	55.92	88.78
P9	91.98	86.75	82.66	93.19	92.57	81.94	64.40	90.53
P10	95.12	93.10	90.55	96.14	94.88	92.03	73.92	93.46
Mean	93.39	91.54	83.56	94.52	93.42	86.78	68.43	91.27
Std.	1.71	2.56	3.89	1.45	1.88	4.50	7.18	1.95

The one-sigma interval of the long-term prediction models for all participants is depicted in Fig. 6 with respect to the prediction steps (horizon). The standard deviation is computed for the participants with respect to the mean values for a given value of step ahead predictions. It can be noted that the predictions are quite smooth, and that the width of the interval gradually increases with the prediction step (*i.e.* toward the end of the prediction period).

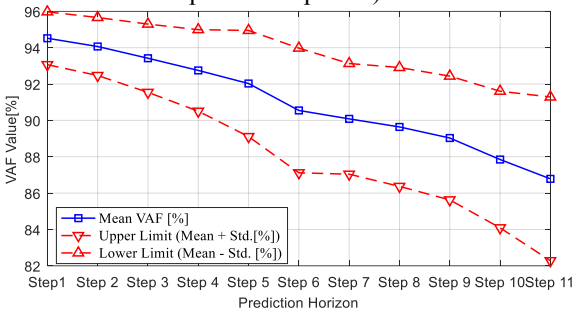

Fig. 7 One sigma interval for multistep LLNF-NARMAX prediction with respect to the prediction horizons for all participants.

On the other hand, in order to investigate the performance of the proposed models, a comparison has been made with respect to the results of different nonlinear modelling methods available in the literature on this recently developed nonlinear system identification benchmark. To this aim,

Table 3 summarizes the results of nonlinear modelling methods proposed by Tian and his co-workers (Tian et al., 2018), where a NARMAX framework based Hierarchical Neural Network (NARMAX-HNN), a Polynomial NARMAX (NARMAX-NP), and a Volterra models were exploited. As it can be seen, the proposed LLNF-NARMAX model (94.52% ±1.45%) generates better results when compared to both NARMAX-HNN (92.33% ±1.57%) and NARMAX-NP (93.91% ±1.54 %) for one-step ahead prediction. In addition, the long-term prediction results given by both LLNF-NARX and LLNF-NARX model are significantly better than the NARMAX-HNN (69.35% ±11.90%) and the NARMAX-NP (47.09% ±13.28%) models. It is also worth highlighting that in contrast to smooth predictions resulted by the proposed LLNF models, abrupt changes are observed with respect to forecasting period in the predictions generated by the NARMAX-HNN and the NARMAX-NP predictor models. Note also that no simulation results were presented by Tian and co-workers (Tian et al., 2018) and the proposed LLNF-based Volterra model greatly outperforms the corresponding structure presented in this work.

Table 3. Performances for the NARMAX-HNN, the polynomial NARMAX (NARMAX-NP), and the Volterra models based on the VAF [%] index (Tian et al., 2018).

	NARMAX-HNN		NARMAX-NP		Volterra
	Step-1	Step-3	Step-1	Step-3	
P1	94.37	63.44	95.52	57.08	38.37
P2	92.83	56.85	94.74	39.53	29.12
P3	90.95	67.16	92.95	31.17	32.18
P4	91.02	74.89	91.94	32.26	28.10
P5	92.58	82.31	94.04	61.57	53.74
P6	93.76	75.55	93.72	49.18	61.07
P7	93.08	74.32	95.73	65.35	54.30
P8	90.23	43.40	91.90	32.57	39.95
P9	90.36	77.16	92.24	37.98	26.35
P10	94.15	78.44	96.28	64.21	65.19
Mean	92.33	69.35	93.91	47.09	42.84
Std.	1.57	11.90	1.54	13.28	13.78

5. CONCLUSION

In this paper, an automatic procedure for the data-driven nonlinear modelling of neurobiological human nervous system on the basis of prediction and simulation techniques was presented. In particular, the local linear neuro-fuzzy architectures that were used to model the cortical response showed several and interesting advantages with respect to conventional black-box approaches, such as neural networks. Moreover, its transparent architecture allowed for more detailed interpretations of the highly nonlinear relationship between the mechanical stimulus and cortical response. The combination of prior knowledge about the human nervous system with measured identification data was also included. The local linear neuro-fuzzy structures of the presented prediction models also provided smooth predictions over forecasting period, when compared to neural network based models. Using the developed models for health monitoring/diagnostic of movement disorders and rehabilitation may constitute a worthwhile direction of future research.

REFERENCES

Billings, S. A. (2013). Nonlinear system identification: NARMAX Methods in the Time, Frequency, and Spatio-Temporal Domains. Chichester: John Wiley & Sons, Ltd.

Breakspear, M. (2017). Dynamic models of large-scale brain activity. *Nat. Neurosci*. 20, 340–352.

Campfens, S. F., Schouten, A. C., Putten, M. J. A. M., and Kooij, H. V. (2013). Quantifying connectivity via efferent and afferent pathways in motor control using coherence measures and joint position perturbations. *Experimental brain research*, 228, 141-153.

Eduardo, M. A., Mendes, M., Billings, S. A. (2001) An Alternative Solution to the Model Structure Selection Problem. *IEEE Transactions on Systems, Man, and Cybernetics—Part A: Systems and Humans*, (31)6, 597.

Nelles O. (2001) *Nonlinear System Identification: From Classical Approaches to Neural Networks and Fuzzy Models*. Springer Press.

Nelles O, Isermann R. (1996). Basis function networks for interpolation of local linear models. Proceedings of IEEE Conference on Decision and Control, Japan, 470–475.

Nozari, H. A., Banadaki, H. D. (2014). Intelligent computationally efficient modelling of multi-input multi-output non-linear dynamical process plants: An industrial steam generator case study. *Proc IMechE Part I: J Systems and Control Engineering*. 228(5), 278–294.

Stone M. (1974). Cross-validatory choice and assessment of statistical predictions. *J. Royal Stat. Soc*., 36(2), 111–147.

Tian, R., Yang, Y., Van der Helm, F. C. T., Dewald, J P. A. (2018). A Novel Approach for Modeling Neural Responses to Joint Perturbations Using the NARMAX Method and a Hierarchical Neural Network. *Frontiers in Computational Neuroscience*, 12, 1-8.

Vlaar, M. P., Birpoutsoukis, G., Lataire, J., Schoukens, M., Schouten, A. C.,Schoukens, J., et al. (2018). Modeling the nonlinear cortical response in EEG evoked by wrist joint manipulation. *IEEE Trans. Neural Syst. Rehabil. Eng*. 26, 205–215.

Vlaar, M. P., Solis-Escalante, T., Vardy, A. N., Van Der Helm, F. C., and Schouten, A. C. (2017). Quantifying nonlinear contributions to cortical responses evoked by continuous wrist manipulation. *IEEE Trans. Neural Syst. Rehabil. Eng*. 25, 481–491.

Yang, Y., Solis-Escalante, T., Van Der Helm, F. C., and Schouten, A. C. (2016b). A generalized coherence framework for detecting and characterizing nonlinear interactions in the nervous system. *IEEE Trans. Biomed. Eng*. 63, 2629–2637.

Yang, Y., Solis-Escalante, T., Yao J., Daffertshofer, A., Schouten A. C., and Helm F. C. (2016a). A General approach for Quantifying Nonlinear Connectivity in the Nervous System Based on Phase Coupling. *International Journal of Neural Systems*, 26, 1550031.